metals

MDPI

Communication

Laser-Induced Iridescent Steel Surfaces with Moderate Reflectance

Xuyang Wang [1], Zhongjia Huang [2] and Xinying Shi [1,*]

[1] School of Physics and Electronic Engineering, Jiangsu Normal University, Xuzhou 221116, China
[2] Anhui Key Laboratory of High-Performance Non-Ferrous Metal Materials, Anhui Polytechnic University, Wuhu 241000, China
* Correspondence: xshi@jsnu.edu.cn

Abstract: Laser-induced coloration on metallic surfaces has emerged as a clean technology to prepare visual designs. After laser processing, the metallic surface is covered by typical periodically repeated microstructures, which interact with visible light and bring iridescent appearance to the laser markings due to the structural color effect. Although many studies have focused on this topic, the necessity of iridescent surfaces with moderate optical reflectance still needs to be addressed. In general, structural colors are shiny with high brightness. There are troubles in certain cases because shiny markings with excessive reflectance may be harmful to human eyes. In this work, we prepared iridescent an AISI444 stainless steel surface via femtosecond laser processing. By studying the influence of surface microstructures on the coloration and reflectance, suitable laser parameters for producing markings with moderate reflectance were discussed. The contribution of intrinsic colors of the chemical compositions in the surface was further analyzed.

Keywords: laser coloration; laser marking; reflectance; surface engineering

Citation: Wang, X.; Huang, Z.; Shi, X. Laser-Induced Iridescent Steel Surfaces with Moderate Reflectance. *Metals* **2023**, *13*, 545. https://doi.org/10.3390/met13030545

Academic Editor: Marcello Cabibbo

Received: 14 February 2023
Revised: 4 March 2023
Accepted: 6 March 2023
Published: 8 March 2023

1. Introduction

Pulsed lasers have been widely employed to modify metallic surfaces and introduce versatile functionalities [1–3]. For example, they can prepare anticorrosive surfaces on steel and aluminum substrates [4,5], endow superhydrophobic features to traditional metal surfaces [5,6], improve mechanical properties and biocompatibility [7], and generate various colors for visual designs [8–10]. Among the aforementioned applications, laser marking on metal and alloy surfaces has emerged as a novel method to make visual designs in both the laboratory and industrial occasions [11,12]. Conventional chemical and electrochemical methods to colorize metallic surfaces inevitably bring environmental pollution [13]. To solve this problem, laser coloration has become favorable with the development of nano- and femtosecond lasers [2].

The current understanding of the laser marking mechanism mainly includes two aspects: the structural colors due to the interactions between visible light and laser-induced periodic surface structures (LIPSS) and nanoparticles (NP) [14–16] and the intrinsic colors contributed by metal oxides and other composites on the surface [10,17]. After laser processing, a thin layer is formed with LIPSS microstructures and a reconstructed compositional distribution. Femtosecond lasers create LIPSS typically on the nanoscale so that the structural color effect is dominant [14,18,19]. Comparatively, nanosecond lasers usually produce surface structures on the micrometer scale, leading to weak light interference, and hence, the appearance would be mainly determined by intrinsic colors of the chemical species on the outer layer [10]. The NPs contribute to the coloration by plasmonic effects, depending on the specific chemical compositions of the NPs and substrates [8,14]. Overall, laser-marking technology offers a controllable way of surface coloration without releasing chemical pollutants. However, laser-processed metallic surfaces sometimes exhibit excessive visible light reflectance [8,20], which cause a new type of light pollution in certain cases.

For example, company logos and visual art designs with laser-induced high-reflectance iridescent appearances are harmful to human eyes, especially in urban regions and indoor situations [21,22]. Therefore, it is necessary to further develop laser-marking technology to produce iridescent surfaces with moderate optical reflectance.

In this work, we studied femtosecond laser-processed AISI444 stainless steel surfaces. Typical LIPSS microstructures were formed on the surface, and their typical sizes were changeable via different laser processing parameters. The color appearance was iridescent at different observation angles, and the brightness was also different among the samples. Such optical properties were further analyzed by measuring the reflectance through spectrophotometry. The reflectance intensity varied due to their LIPSS differences. We discussed suitable laser parameters for preparing steel surfaces with moderate reflectance. The detailed coloration mechanism was interpreted by comparing the appearance and reflectance and quantitative analysis of intrinsic color contributions. We hope this work will be helpful in the practical application of femtosecond laser marking.

2. Experimental

Commercial AISI444 stainless steel contains the main alloying element of Cr up to 17.5~19.5% and other alloying elements (Mn, Ni, etc.) below 1%. Steel samples were mechanically polished and then irradiated by a femtosecond laser with the pulse length of 293 fs. During laser processing, laser pulses were focused on steel surfaces with the pulse energy of 0.64 μJ. After laser irradiation, the sizes of laser-induced craters were measured. We found the crater size varied due to different laser fluencies, and the focused beam had a radius of 8 μm. The damage threshold energy was calculated as 0.1 μJ for a single-laser pulse on the surface of steel samples [23]. The damage threshold fluency for a single pulse could thus be calculated as 0.09 J/cm^2. The laser wavelength, fluency, and laser pulse pitch were varied for different samples, as shown in Table 1. These above laser parameters were chosen according to multiple trials of laser treatments. Based on the fluencies in Table 1, the fluencies employed in the processing were 69 or 147 times greater than the damage threshold. Considering that the pulse pitches in Table 1 are comparable to the laser beam size, we can conclude that each crater is affected by only a very small proportion of the pulses. It therefore results in very limited overlapping. The laser pulse repetition rate was fixed to 885 Hz, which has been proven as suitable for stainless steel [14]. The low repetition rate is helpful to limit heat accumulation. During laser processing, the steel samples were moved laterally so that individual laser pulses reached the steel surfaces at an even pitch width.

Table 1. Laser processing parameters.

Samples	Laser Wavelength (nm)	Fluency (J/cm^2)	Pulse Pitch (μm)
Sample 1	1040	13.22	3.2
Sample 2	1040	6.25	3.2
Sample 3	520	13.22	2.2
Sample 4	520	6.25	3.2

The morphologies of the steel surfaces after laser processing were examined through a Hitachi SU8010 field-emission scanning electron microscope (FESEM) equipped with an energy-dispersive spectrometer (EDS) for elemental analysis. The appearance and colors were recorded by a digital camera under natural light illumination. The surface brightness was evaluated by the gloss intensity, which was measured by an Elcometer 480 glossmeter using the mode of a 60° angle [24,25]. Gloss measurement is based on the amount of light reflected on the surface and is measured in Gloss Units (GU). The optical properties, including the reflectance and refractory indices, were measured by a Lambda 950 UV-Vis spectrophotometer and a Horiba Jobin-Yvon ellipsometer. The elemental identification and chemical states were quantitatively investigated through a Thermo Fisher K-Alpha X-ray photoelectron spectroscope (XPS). In addition to the survey scan for elemental

identification, high-resolution scans were performed especially for Fe, Cr, and other alloy elements in steel. Prior to fitting the XPS spectra, the data were calibrated with the 1 s peak of adventitious carbon.

3. Results and Discussion

3.1. Surface Structures and Coloration Appearance

The SEM images of the four laser-processed AISI444 stainless steel samples are shown in Figure 1. The steel surface was reconstructed due to the femtosecond second laser irradiation. Among the four samples, the morphologies of Samples 1 and 2 exhibit slightly interrupted LIPSSs. Although these two samples have a similar LIPSS appearance, their specific sizes are slightly distinct due to the different fluencies employed [26]. The average ripple width and structure repetition width of Sample 1 are 440 nm and 800 nm, respectively. The lower fluency resulted in slightly larger sizes for Sample 2, which are 460 nm for the ripple width and 910 nm for the repetition width. The LIPSS of Sample 3 is well distributed and it has the smallest surface structures, which are 275 nm and 430 nm for the ripple and repetition widths, respectively. This was expected because of the higher fluency and narrower laser pulse pitch. Processed with the same laser wavelength but a lower fluency and a larger pulse pitch than Sample 3, Sample 4 has a medium size, and its ripple and repetition widths are 370 nm and 790 nm.

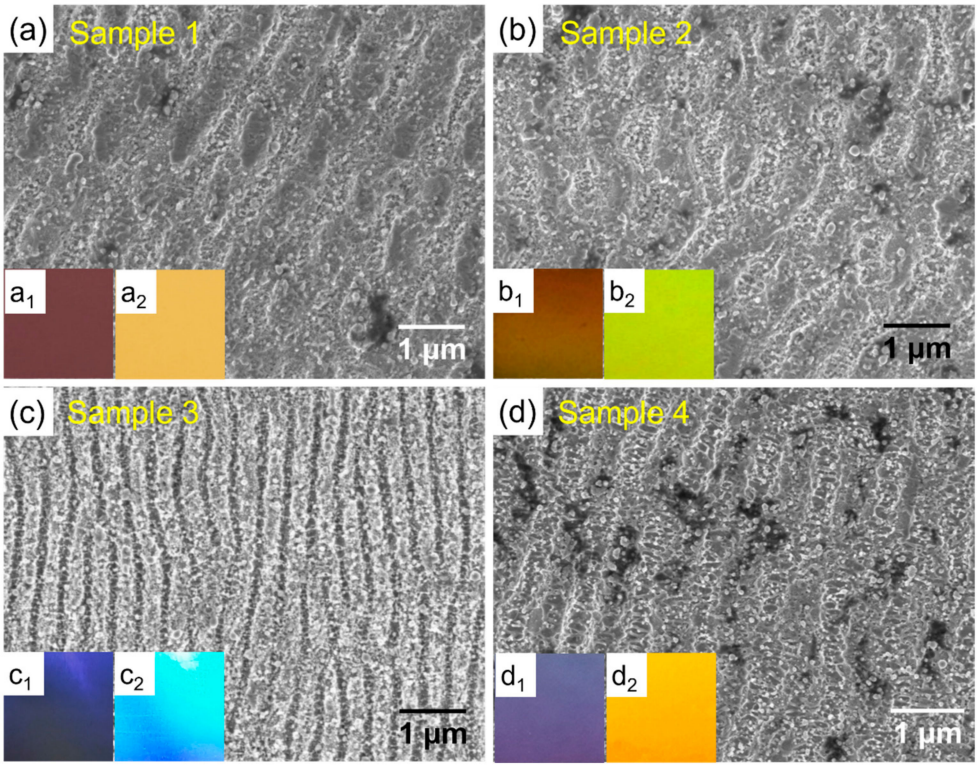

Figure 1. Morphologies and angle-dependent appearances of laser-marked steel surfaces. (**a**–**d**) SEM images of the Samples 1–4, and the insets in each panel are optical photos taken at the angles of 30 and 70 degrees, respectively.

Laser irradiation also brings typical coloration on steel surfaces, which are shown in the insets of each panel in Figure 1. The insets of each panel were observed by a digital camera at the angles of 30 and 70 degree, respectively. It can be seen that the iridescent photos are angle dependent, which suggests an obvious structural color effect. Samples 1 and 2 exhibit similar structural colors because of their similar LIPSS sizes. Sample 3 looks the shiniest among all the samples. It should be attributed to the smallest structure size, which involves the greatest light–matter interference. The nanoparticles may also

contribute to the coloration through the plasmonic effect; however, such an effect may be quite limited according to previous research with 301LN steel [14]. The brightness of the photos could also suggest different intensities of optical reflectance. Surface gloss was measured to evaluate the brightness, and the results are listed in Table S1. According to the gloss categories (>70 GU, high gloss; 10~70 GU, semigloss; <10 GU, low gloss), Samples 1 and 2 exhibit medium gloss, Sample 3 shows high gloss, and Sample 4 has a gloss slightly lower than Sample 3.

3.2. Optical Properties

In order to investigate the correlation between the shiny appearance and optical reflectance, the laser-marked samples were measured through UV-Vis spectrophotometry with the incident angle of 70 degrees. Figure 2 shows the visible light reflectance (300~800 nm). All spectra have obvious peaks which are in accordance with the colors shown in the insets labelled as x_2 (x represents a–d) in Figure 1. For example, the reflectance peak of Sample 3 at around 400 nm matches the shiny blue color of the photo in the c_2 inset.

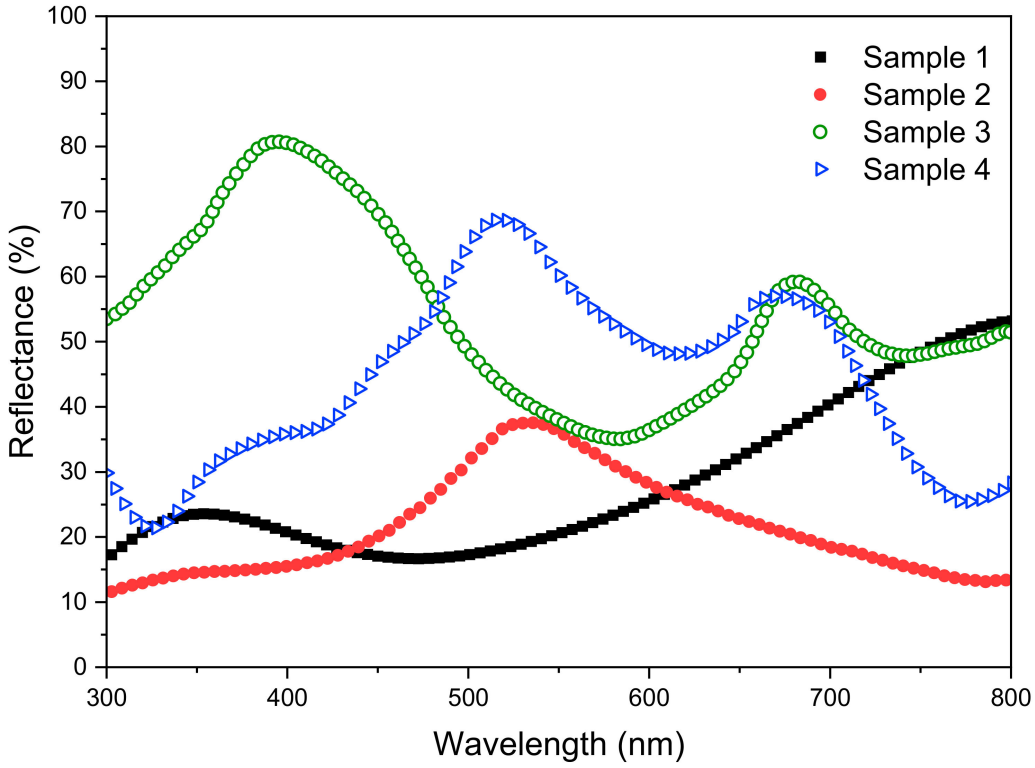

Figure 2. Optical reflectance of laser-processed steel samples.

Among the reflectance spectra, Samples 1 and 2 have a relatively low reflectance below 30% in most of the wavelength range. Sample 3 shows the highest reflectance value which is above 35% in the whole range and up to 80% at 400 nm. The reflectance of Sample 4 is also very high within the range of 420~700 nm. It can be seen that both Samples 3 and 4 exhibit high reflectance, and their surface structures are formed under the irradiation of a lower laser wavelength (520 nm). In contrast, laser processing with a 1040 nm wavelength leads to a relatively lower reflectance and also obvious iridescent colors. Therefore, such laser processing conditions are suitable for preparing eye-friendly markings, especially for stainless steel surfaces [27].

3.3. Coloration Mechanism

The iridescent appearance in Figure 1 indicates that the structural color effect has great effect on surface coloration. However, it is still necessary to examine the contribution of

intrinsic colors of the chemical compositions on the steel surface [28]. EDS results show that Fe and Cr are the main elements of both the original AISI444 steel substrates and the laser-marked regions. However, EDS is incompetent to identify the chemical compounds, and the results are usually interrupted by the original steel substrates due to the large detection depth [10]. In this case, the surface-sensitive XPS technique was carried out to identify the chemical species and quantify their relative contents. Samples 1 and 2 were characterized considering their moderate optical reflectance. Since Fe and Cr were the main contents of the steel samples, the Fe 2*p* and Cr 2*p* spectra were particularly well fitted, as shown in Figure 3.

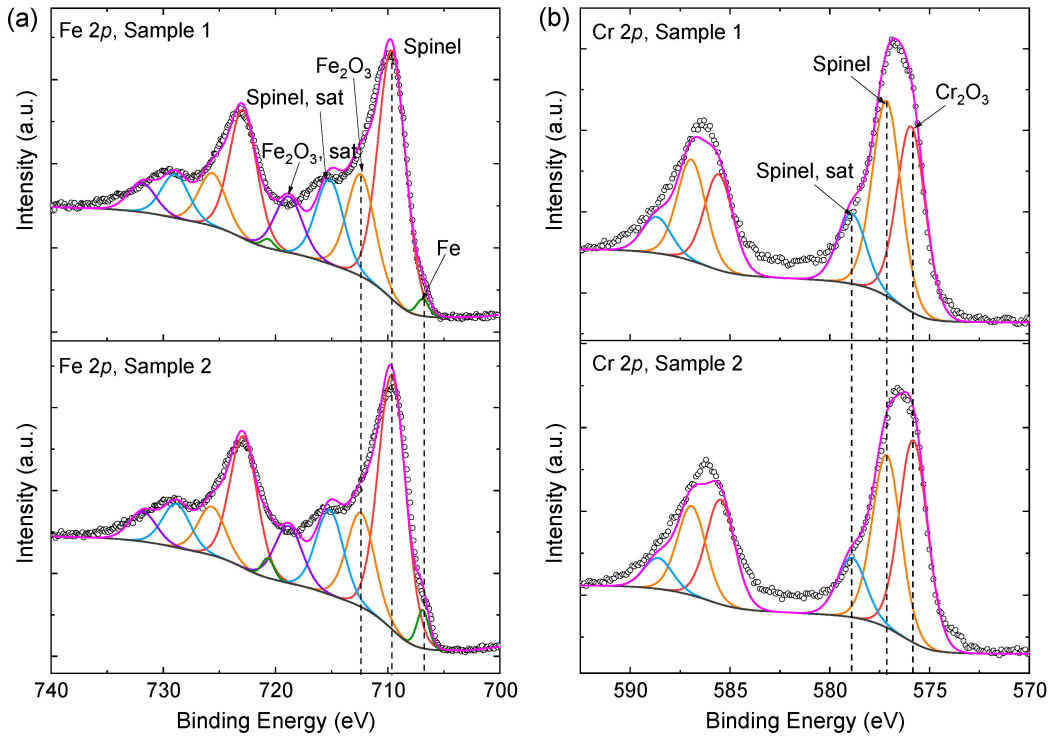

Figure 3. XPS spectra of the steel samples after laser processing. (**a**) Fe 2*p* spectra; (**b**) Cr 2*p* spectra. The identified species were marked for $2p_{3/2}$ peaks.

The chemical compositions of the steel samples were changed during laser ablation, and the compositions usually exhibit intrinsic colors, which also influence the surface coloration. By fitting the XPS spectra, Fe metal, Fe_2O_3, and a complicated spinel were identified in Figure 3a and Cr_2O_3 and a spinel in Figure 3b. The binding energy, the full width at half maximum (FWHM), and the normalized atomic contents of the fitted components are listed in Table 2. The relative contents of the identified chemicals could be further calculated based on Table 2. It was found that the spinel takes 65.30% and 64.49% of the surfaces of Samples 1 and 2. The spinel has a common chemical formula of XY_2O_4, where X and Y represent oxidized metallic ions with +2 and +3 valences, respectively. Since the minor alloying elements (Mn, Ni, etc.) were not taken into account in this study, X and Y could be specified as Fe^{2+} and $Fe^{3+}Cr^{3+}$, respectively [29]. The relative contents of Fe, Fe_2O_3, and Cr_2O_3 were also calculated, which are 1.23%, 25.91%, and 7.56% for Sample 1 and 2.70%, 24.68%, and 8.13% for Sample 2, respectively. Such quantification results suggest that the two samples have a very similar chemical composition.

Table 2. Fe 2*p* and Cr 2*p* peak-fitting results.

Valence States	Samples	Components	Binding Energy (eV)	FWHM (eV)	Normalized Atomic Percentage (%)
Fe 2*p*	Sample 1	Fe	706.88	1.25	1.23
		Spinel-Fe	709.62	2.88	40.64
		Fe_2O_3	712.40	2.88	16.70
		Spinel-Fe, sat	715.17	2.88	13.81
		Fe_2O_3, sat	718.84	2.88	9.22
	Sample 2	Fe	706.88	1.25	2.70
		Spinel-Fe	709.62	2.88	41.36
		Fe_2O_3	712.40	2.88	15.34
		Spinel-Fe, sat	715.17	2.88	13.79
		Fe_2O_3, sat	718.84	2.88	9.34
Cr 2*p*	Sample 1	Cr_2O_3	575.93	1.68	7.56
		Spinel-Cr	577.15	1.68	7.99
		Spinel-Cr, sat	578.90	1.68	2.86
	Sample 2	Cr_2O_3	575.81	1.68	8.11
		Spinel-Cr	577.15	1.68	6.93
		Spinel-Cr, sat	578.90	1.68	2.41

The distribution of the aforementioned chemical compositions on steel surfaces is relative to the coloration. Through the EDS mapping of the Fe and Cr elements of Sample 3 (Figure S1), it could be found that Fe and Cr are almost evenly distributed. However, it is difficult to examine the distribution of those chemical compounds, i.e., Fe_2O_3, Cr_2O_3, and the spinel compound. Considering the EDS results and previous research [10,14], the chemicals are supposed to be evenly distributed in the laser-marked layer. Their intrinsic colors in the RGB model could be determined from previous reports [10,30], which are (130, 110, 90), (80, 121, 95), and (210, 90, 165) for Fe_2O_3, Cr_2O_3, and the spinel compound, respectively. Computed by the product of the composition matrix and color matrix [14], the intrinsic RGB colors of the two samples are (177, 88, 138) and (174, 86, 136), which could be named as "rose quartz pink" [31] and are difficult to distinguish by human eyes.

It can be found that the main chemical compositions have unsaturated colors, and the calculated intrinsic colors are also medium for the R, G, and B values. Such intrinsic colors would interact with the structural coloration, which is beneficial to adjust the surface coloration and avoid strong shiny appearances. Regarding the structural color effect, well-distributed LIPSSs with smaller sizes would be more likely to exhibit shiny colors and high reflectance. Considering the synergistic effect of structural and intrinsic colors, applicable laser-induced steel surfaces should have suitable LIPSS sizes to generate iridescent colors and certain chemical compositions with intrinsic colors to tune the surface appearance. In this study, Samples 1 and 2 have medium LIPSS sizes, and the ripples are not so well distributed compared to Sample 3. The surfaces thus show mild colors, which suggests a medium structural color effect. The unsaturated intrinsic colors also contribute to the surface appearance and help to regulate both the coloration and reflectance intensity, especially in the case of a mild structural color effect.

4. Conclusions

In summary, we have prepared typical LIPSSs on AISI444 stainless steel surfaces through femtosecond laser processing. The laser markings are iridescent, which is primarily attributed to the structural color effect. We have noticed that the tunable visible light reflectance is related to the LIPSS sizes and laser parameters. With a ripple width larger than 460 nm and a repetition width above 910 nm, the visible light reflectance is restricted below 40%. Relatively low-intensity reflection is favorable in many applications. Therefore, we chose Samples 1 and 2 for further analysis of intrinsic color contributions. By quantifying the chemical compositions and calculating the intrinsic colors, we found that intrinsic colors

with medium RGB values are necessary to adjust the coloration. Therefore, tunable and medium-reflectance steel surfaces could be fabricated via the experimental conditions provided in this work. Such a strategy involves the analysis of specific chemical contents and the calculation of intrinsic colors, which would be also applicable to other metals and alloys. In addition, the application of femtosecond laser processing may also make it possible to create secure marks, e.g., copyright marks, in ultraviolet or infrared, which is thus invisible to human eyes.

Supplementary Materials: The following supporting information can be downloaded at: https://www.mdpi.com/article/10.3390/met13030545/s1, Figure S1: EDS mapping of the Fe and Cr elements of Sample 3; Table S1: Surface gloss results of the samples.

Author Contributions: X.W.—investigation, characterization, and writing—original draft. Z.H.—investigation. X.S.—supervision and writing—review and editing. All authors have read and agreed to the published version of the manuscript.

Funding: This work was financially supported by the National Natural Science Foundation of China (No. 61904069), the Natural Science Foundation of Jiangsu Higher Education Institutions of China (No. 19KJB140008), and the Anhui Provincial Natural Science Foundation (No. 2008085ME141).

Acknowledgments: M.J. Laakso is acknowledged for help in sample preparation.

Conflicts of Interest: The authors declare no conflict of interest.

References

1. Liu, H.; Lin, W.; Hong, M. Surface coloring by laser irradiation of solid substrates. *APL Photonics* **2019**, *4*, 051101. [CrossRef]
2. Vorobyev, A.Y.; Guo, C. Direct femtosecond laser surface nano/microstructuring and its applications. *Laser Photonics Rev.* **2013**, *7*, 385–407. [CrossRef]
3. Chen, Y.; Newkirk, J.W.; Liou, F. Synthesizing Ti–Ni alloy composite coating on Ti–6Al–4V surface from laser surface modification. *Metals* **2023**, *13*, 243. [CrossRef]
4. Ruzankina, J.S.; Parfenov, V.A.; Vasiliev, O.S. Anti-corrosion prevention of carbon steel by means of laser treatment. *Laser Phys.* **2018**, *29*, 015203. [CrossRef]
5. Yuan, G.; Liu, Y.; Ngo, C.-V.; Guo, C. Rapid fabrication of anti-corrosion and self-healing superhydrophobic aluminum surfaces through environmentally friendly femtosecond laser processing. *Opt. Express* **2020**, *28*, 35636–35650. [CrossRef]
6. Liu, M.; Li, M.-T.; Xu, S.; Yang, H.; Sun, H.-B. Bioinspired superhydrophobic surfaces via laser-structuring. *Front. Chem.* **2020**, *8*, 835. [CrossRef]
7. Zhang, J.; Guan, Y.; Lin, W.; Gu, X. Enhanced mechanical properties and biocompatibility of Mg-Gd-Ca alloy by laser surface processing. *Surf. Coat. Tech.* **2019**, *362*, 176–184. [CrossRef]
8. Guay, J.-M.; Lesina, A.C.; Côté, G.; Charron, M.; Poitras, D.; Ramunno, L.; Berini, P.; Weck, A. Laser-induced plasmonic colours on metals. *Nat. Commun.* **2017**, *8*, 16095. [CrossRef]
9. Andreeva, Y.M.; Luong, V.C.; Lutoshina, D.S.; Medvedev, O.S.; Mikhailovskii, V.Y.; Moskvin, M.K.; Odintsova, G.V.; Romanov, V.V.; Shchedrina, N.N.; Veiko, V.P. Laser coloration of metals in visual art and design. *Opt. Mater. Express* **2019**, *9*, 1310–1319. [CrossRef]
10. Lu, Y.; Shi, X.; Huang, Z.; Li, T.; Zhang, M.; Czajkowski, J.; Fabritius, T.; Huttula, M.; Cao, W. Nanosecond laser coloration on stainless steel surface. *Sci. Rep.* **2017**, *7*, 7092. [CrossRef]
11. Zhao, H.; Zhang, Q.; Hou, Y.; Cheng, Z.; Xia, T.; Cao, S.; Wang, P. Color visual art creation on metals via multifunctional laser paintbrush. *Opt. Laser Technol.* **2023**, *159*, 109040. [CrossRef]
12. Veiko, V.P.; Andreeva, Y.; Cuong, L.V.; Lutoshina, D.; Polyakov, D.; Sinev, D.; Mikhailovskii, V.; Kolobov, Y.R.; Odintsova, G. Laser paintbrush as a tool for modern art. *Optica* **2021**, *8*, 577–585. [CrossRef]
13. Taveira, L.V.; Kikuti, E.; Bocchi, N.; Dick, L.F. Microcharacterization of colored films formed on AISI 304 by different electrochemical methods. *J. Electrochem. Soc.* **2006**, *153*, B411–B416. [CrossRef]
14. Shi, X.; Huang, Z.; Laakso, M.J.; Niklaus, F.; Sliz, R.; Fabritius, T.; Somani, M.; Nyo, T.; Wang, X.; Zhang, M.; et al. Quantitative assessment of structural and compositional colors induced by femtosecond laser: A case study on 301LN stainless steel surface. *Appl. Surf. Sci.* **2019**, *484*, 655–662. [CrossRef]
15. Garcell, E.M.; Singh, S.C.; Li, H.; Wang, B.; Jalil, S.A.; Guo, C. Comparative study of femtosecond laser-induced structural colorization in water and air. *Nanoscale Adv.* **2020**, *2*, 2958–2967. [CrossRef]
16. Sun, H.; Li, J.; Liu, M.; Yang, D.; Li, F. A review of effects of femtosecond laser parameters on metal surface properties. *Coatings* **2022**, *12*, 1596. [CrossRef]
17. Phillips, K.C.; Gandhi, H.H.; Mazur, E.; Sundaram, S.K. Ultrafast laser processing of materials: A review. *Adv. Opt. Photonics* **2015**, *7*, 684–711. [CrossRef]

18. Yin, K.; Wang, C.; Duan, J.; Guo, C. Femtosecond laser-induced periodic surface structural formation on sapphire with nanolayered gold coating. *Appl. Phys. A* **2016**, *122*, 834. [CrossRef]
19. Luo, Z.; Duan, J.; Guo, C. Femtosecond laser one-step direct-writing cylindrical microlens array on fused silica. *Opt. Lett.* **2017**, *42*, 2358–2361. [CrossRef]
20. Guo, T.; Liu, Z.; Jin, Y.; Wang, N.; Zhang, Z.; He, S. Large-scale panchromatic structural color manipulation via thermal trimming. *Adv. Opt. Mater.* **2021**, *10*, 2101546. [CrossRef]
21. Adams, C.A.; Fernández-Juricic, E.; Bayne, E.M.; St. Clair, C.C. Effects of artificial light on bird movement and distribution: A systematic map. *Environ. Evid.* **2021**, *10*, 37. [CrossRef]
22. Kowalska, J. Coloured light pollution in the urban environment. *Photonics Lett. Pol.* **2019**, *11*, 93–95. [CrossRef]
23. Pietroy, D.; Maio, Y.D.; Moine, B.; Baubeau, E.; Audouard, E. Femtosecond laser volume ablation rate and threshold measurements by differential weighing. *Opt. Express* **2012**, *20*, 29900–29908. [CrossRef] [PubMed]
24. Ulbrich, D.; Kowalczyk, J.; Jósko, M.; Sawczuk, W.; Chudyk, P. Assessment of Selected Properties of Varnish Coating of Motor Vehicles. *Coatings* **2021**, *11*, 1320. [CrossRef]
25. Hodgson, S.D.; Waugh, D.G.; Gillett, A.; Lawrence, J. High speed CO_2 laser surface modification of iron/cobalt co-doped boroaluminosilicate glass and the impact on surface roughness, gloss and wettability. *Laser Phys. Lett.* **2016**, *13*, 076102. [CrossRef]
26. Rohloff, M.; Das, S.K.; Höhm, S.; Grunwald, R.; Rosenfeld, A.; Krüger, J.; Bonse, J. Formation of laser-induced periodic surface structures on fused silica upon multiple cross-polarized double-femtosecond-laser-pulse irradiation sequences. *J. Appl. Phys.* **2011**, *110*, 014910. [CrossRef]
27. Gnilitskyi, I.; Gruzdev, V.; Bulgakova, N.M.; Mocek, T.; Orazi, L. Mechanisms of high-regularity periodic structuring of silicon surface by sub-MHz repetition rate ultrashort laser pulses. *Appl. Phys. Lett.* **2016**, *109*, 143101. [CrossRef]
28. Cucerca, S.; Didyk, P.; Seidel, H.-P.; Babaei, V. Computational image marking on metals via laser induced heating. *ACM Trans. Graph.* **2020**, *39*, 70. [CrossRef]
29. Biagioni, C.; Marco, P. The systematics of the spinel-type minerals: An overview. *Am. Mineral.* **2014**, *99*, 1254–1264. [CrossRef]
30. Torrent, J.; Barrón, V. Diffuse reflectance spectroscopy of iron oxides. *Encycl. Surf. Colloid Sci.* **2002**, *1*, 1438–1446.
31. Color-Name. Available online: https://www.color-name.com/ (accessed on 1 February 2023).